iScience

CellPress
OPEN ACCESS

Article

MiR-337-3p improves metabolic-associated fatty liver disease through regulation of glycolipid metabolism

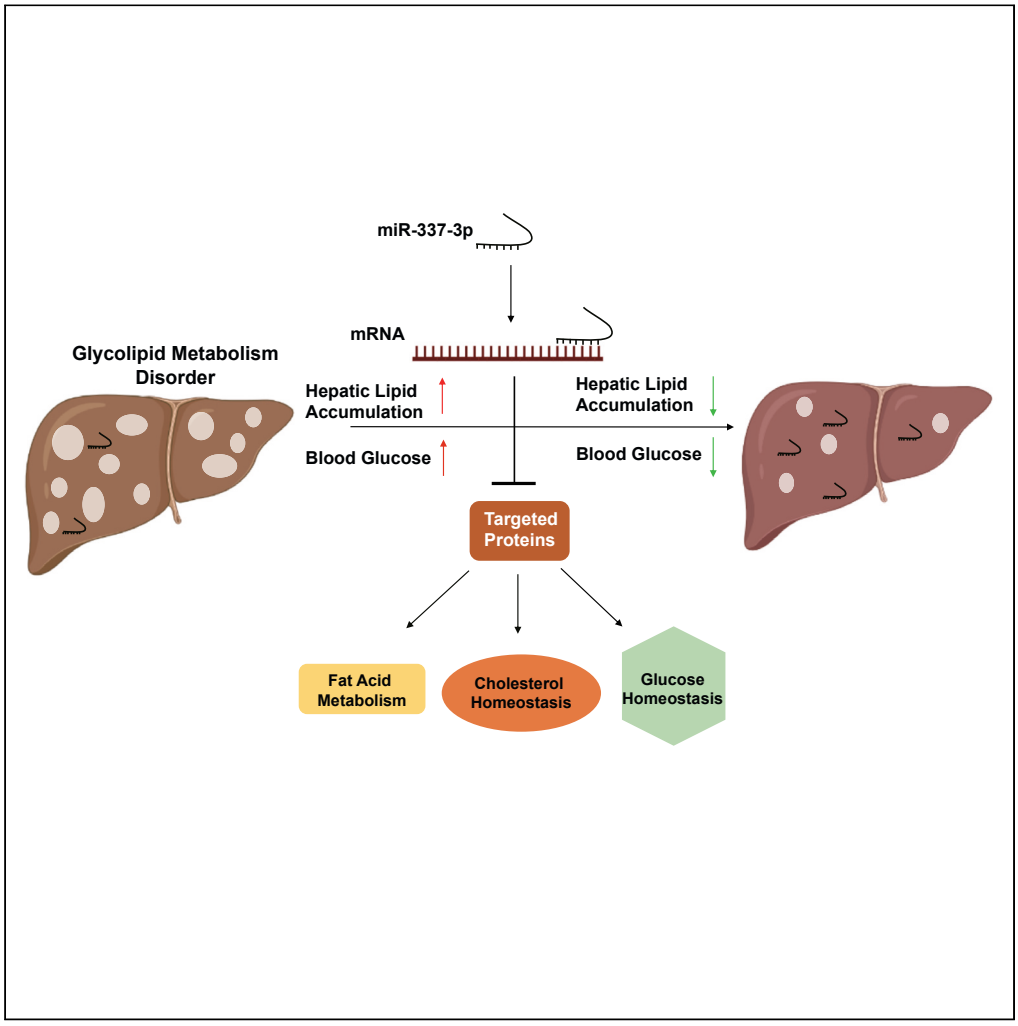

Xiaoding Xu, Chuwei Yu, Hongxiu He, ..., Likun Gong, Jing Chen, Jin Ren

jingchen@simm.ac.cn (J.C.)
jren@cdser.simm.ac.cn (J.R.)

Highlights

MiR-337-3p is decreased in NAFLD patients and corresponding mouse models

Overexpression of miR-337-3p improved lipid and glucose metabolism in mouse models

MiR-337-3p regulated metabolism via multiple targets

Xu et al., iScience *26*, 108352
November 17, 2023
https://doi.org/10.1016/j.isci.2023.108352

iScience

CellPress
OPEN ACCESS

Article

MiR-337-3p improves metabolic-associated fatty liver disease through regulation of glycolipid metabolism

Xiaoding Xu,[1,2,3] Chuwei Yu,[2,3] Hongxiu He,[1,2,3] Xiangyu Pan,[2,4] Aijun Hou,[2,3] Jianxun Feng,[2] Rongrong Tan,[2] Likun Gong,[1,2,3] Jing Chen,[1,2,3,5,*] and Jin Ren[1,2,3,*]

SUMMARY

Epigenetic regulations play crucial roles in the pathogenesis of metabolic-associated fatty liver disease; therefore, elucidating the biological functions of differential miRNAs helps us to understand the pathogenesis. Herein, we discovered miR-337-3p was decreased in patients with NAFLD from Gene Expression Omnibus dataset, which was replicated in various cell and mouse models with lipid disorders. Subsequently, overexpression of miR-337-3p *in vivo* could ameliorate hepatic lipid accumulation, reduce fasting blood glucose, and improve insulin resistance. Meanwhile, we determined miR-337-3p might influence multiple genes involved in glycolipid metabolism through mass spectrometry detection, bioinformatics analysis, and experimental verification. Finally, we selected HMGCR as a representative example to investigate the molecular mechanism of miR-337-3p regulating these genes, where the seed region of miR-337-3p bound to 3′UTR of HMGCR to inhibit HMGCR translation. In conclusion, we discovered a new function of miR-337-3p in glycolipid metabolism and that might be a new therapeutic target of MAFLD.

INTRODUCTION

Metabolic-associated fatty liver disease (MAFLD), also known as nonalcoholic fatty liver disease (NAFLD) before, is the most prevalent liver disorder worldwide, affecting one-third of the population.[1,2] It has been a leading cause of liver transplants and hepatocellular carcinoma;[3] however, there is still a lack of effective treatments. The pathogenesis of MAFLD is extremely complex because it is associated with a thorough reprogramming of hepatic metabolism, which leads to impaired glucose homeostasis and lipid accumulation. During this process, the genes involved in controlling glycolipid metabolism are deregulated, which may be caused by the alterations of epigenetic mechanisms that dictate gene expression. As one of the main epigenetic mechanisms, microRNAs (miRNAs) have been proved to play key roles in metabolic disorders.[4]

miRNAs are endogenously transcribed non-coding RNA approximately 22-nt-long, which can regulate gene transcription or translation in a variety of patterns to act as key regulators in many biological processes.[5–9] It is well known that various metabolic pathways in MAFLD, including *de novo* lipogenesis, uptake and export of lipid, lipid oxidation, hepatic glycolysis, gluconeogenesis, and glycogen metabolism, are tightly regulated by specific miRNA.[4] For example, miR-122, which accounts for nearly 70% of miRNA contents in the liver, has been reported to be downregulated significantly in nonalcoholic steatohepatitis (NASH) and target a variety of factors in lipid metabolism, including FASN (the key enzyme of fatty acid synthesis), HMGCR (the key enzyme of cholesterol synthesis), and SREBP-1c and SREBP-2 (the key transcription factors of lipid metabolism),[10] thereby participating in triglyceride (TG) synthesis and secretion, steatohepatitis, fibrosis, etc. Therefore, clarifying the pathophysiological roles of specific miRNA, especially downregulated miRNAs during MAFLD, will help us better understand the pathogenesis of this disease.

MiR-337 gene is localized on chromosome 14q32.2,[9] and miR-337-3p is one of products of this gene. Current evidence indicates that miR-337-3p is downregulated in various human cancer types, such as melanoma,[11] neuroblastoma,[12] colorectal cancer,[13] non-small cell lung cancer,[14] and hepatocellular carcinoma,[15] and plays regulatory roles in some diseases and biological processes, including gastric tumor, breast cancer, osteoarthritis, and hepatic cell differentiation.[16–19] In our lab, we found the relationship between miR-337-3p and low-density lipoprotein cholesterol (LDL-C) in hyperlipidemic mice,[20] which clued us it might also regulate other metabolic process.

[1]School of Chinese Materia Medica, Nanjing University of Chinese Medicine, Nanjing 210023, China
[2]Center for Drug Safety Evaluation and Research, State Key Laboratory of Drug Research, Shanghai Institute of Materia Medica, Chinese Academy of Sciences, 501 Haike Road, Shanghai 201203, China
[3]University of Chinese Academy of Sciences, No.19A Yuquan Road, Beijing 100049, China
[4]Department of Pharmaceutics, College of Pharmaceutical Sciences, Soochow University, Suzhou 215123, P.R. China
[5]Lead contact
*Correspondence: jingchen@simm.ac.cn (J.C.), jren@cdser.simm.ac.cn (J.R.)
https://doi.org/10.1016/j.isci.2023.108352

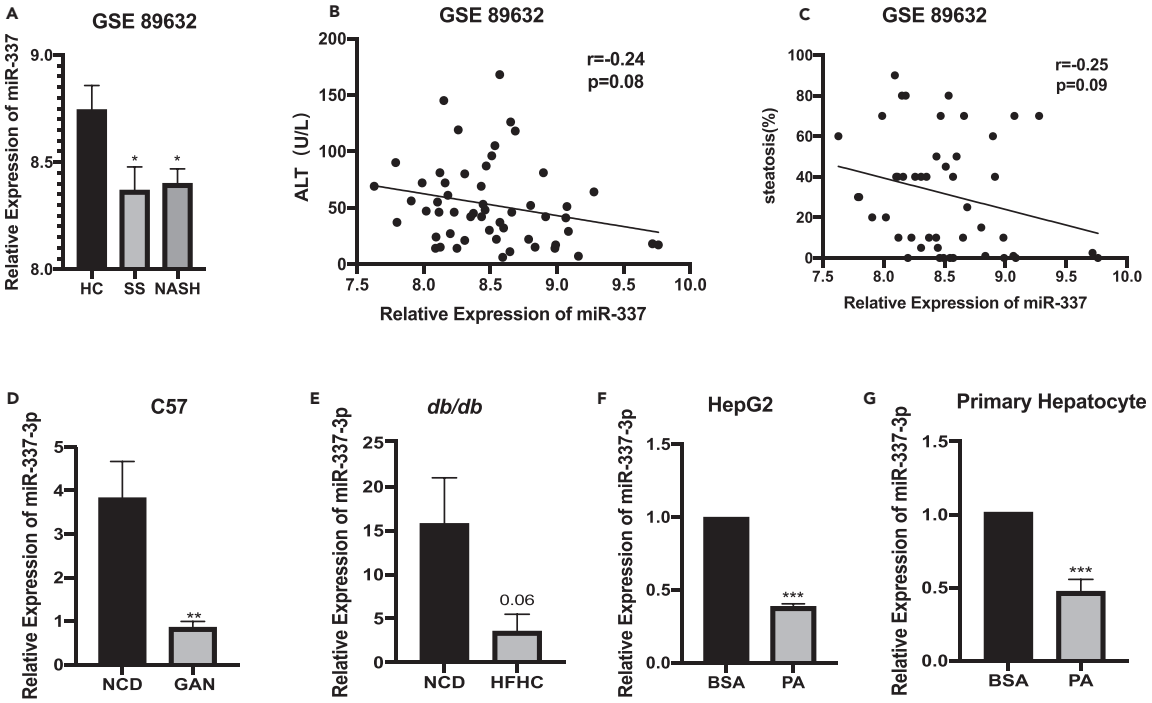

Figure 1. MiR-337-3p is decreased in patients, mouse, and cell models with abnormal lipid metabolism

(A) The level of hepatic miR-337 in GSE89632 (n = 18 in HC, n = 17 in SS, n = 19 in NASH).

(B) The relationship between miR-337 and ALT in GSE89632.

(C) The relationship analysis between miR-337 and steatosis in GSE89632.

(D and E) RT-qPCR analysis of the relative miR-337-3p levels in C57/BL6 fed with normal chow diet (NCD) and GAN diet (n = 10/each group) (D), *db/db* fed with normal chow diet (NCD) and HFHC (n = 5/each group) (E).

(F and G) RT-qPCR analysis of the relative miR-337-3p levels in HepG2 (F) and primary hepatocyte(G) treated with PA. The results of A, B, C, D, and E are presented as mean ± SEM. The results of F and G are presented as mean ± SD. *p < 0.05, **p < 0.01, ***p < 0.001 versus the HC, NCD or BSA group.

In current work, we discovered that miR-337 is downregulated in NAFLD patients and has a negative correlation with the level of alanine transaminase (ALT) and the degree of steatosis. Furthermore, miR-337-3p is obvious lower in multiple cell and mouse models of NAFLD, which drived us to investigate its potential role in NAFLD. After overexpressed in the liver, miR-337-3p could improve glucose and lipid metabolism in different diet-induced mouse models. The potential molecular mechanism further clarified that miR-337-3p might ameliorate the homeostatic effects of lipid and glucose through multitarget inhibition.

RESULT

MiR-337-3p is decreased in NAFLD patients and corresponding cell and mouse models

To investigate whether miR-337 is differentially expressed in clinic, we analyzed the data of GSE89632 which is a cross-sectional study, including patients with non-alcoholic fatty liver disease (20 simple steatosis (SS), 19 NASH) and 24 healthy living liver donors (HC). After removing the patients with fibrotic symptoms in the HC (6 cases) and SS (3 case) groups, we found that miR-337-3p was obviously decreased in SS and NASH groups (Figure 1A) and it had a negative correlation with the level of ALT ($r = -0.24$, $p = 0.08$) and the degree of steatosis on liver biopsy ($r = -0.25$, $p = 0.09$) (Figures 1B and 1C), which suggested that miR-337 might participate in the regulation of hepatic lipid accumulation and liver injury during NAFLD. Subsequently, we confirmed this finding in two mouse models of NAFLD (*db/db* mice fed with a high-fat diet (0.5% cholesterol, 23% fat) and C57 mice fed with a Gubra-Amylin NASH (GAN) diet (40 kcal% fat, 2% cholesterol, 20 kcal% fructose)) and PA-stimulated cell models (HepG2 and mouse primary hepatocytes). As shown in Figures 1D–1G, miR-337-3p levels in model groups were significantly lower than those in the corresponding control group.

Taken together, miR-337-3p is downregulated in clinical patients and multiple NAFLD models, suggesting that this decline may be involved in the pathogenesis of NAFLD.

Overexpression of miR-337-3p alleviated hepatic steatosis, inflammation, and fibrosis in GAN diet-induced mice

The previously described results aroused our interests in examining the potential role of miR-337-3p during NAFLD. Adeno-associated virus-mediated liver-directed miRNA overexpression was used to investigate the effect of miR-337-3p on NAFLD-associated pathologies in the

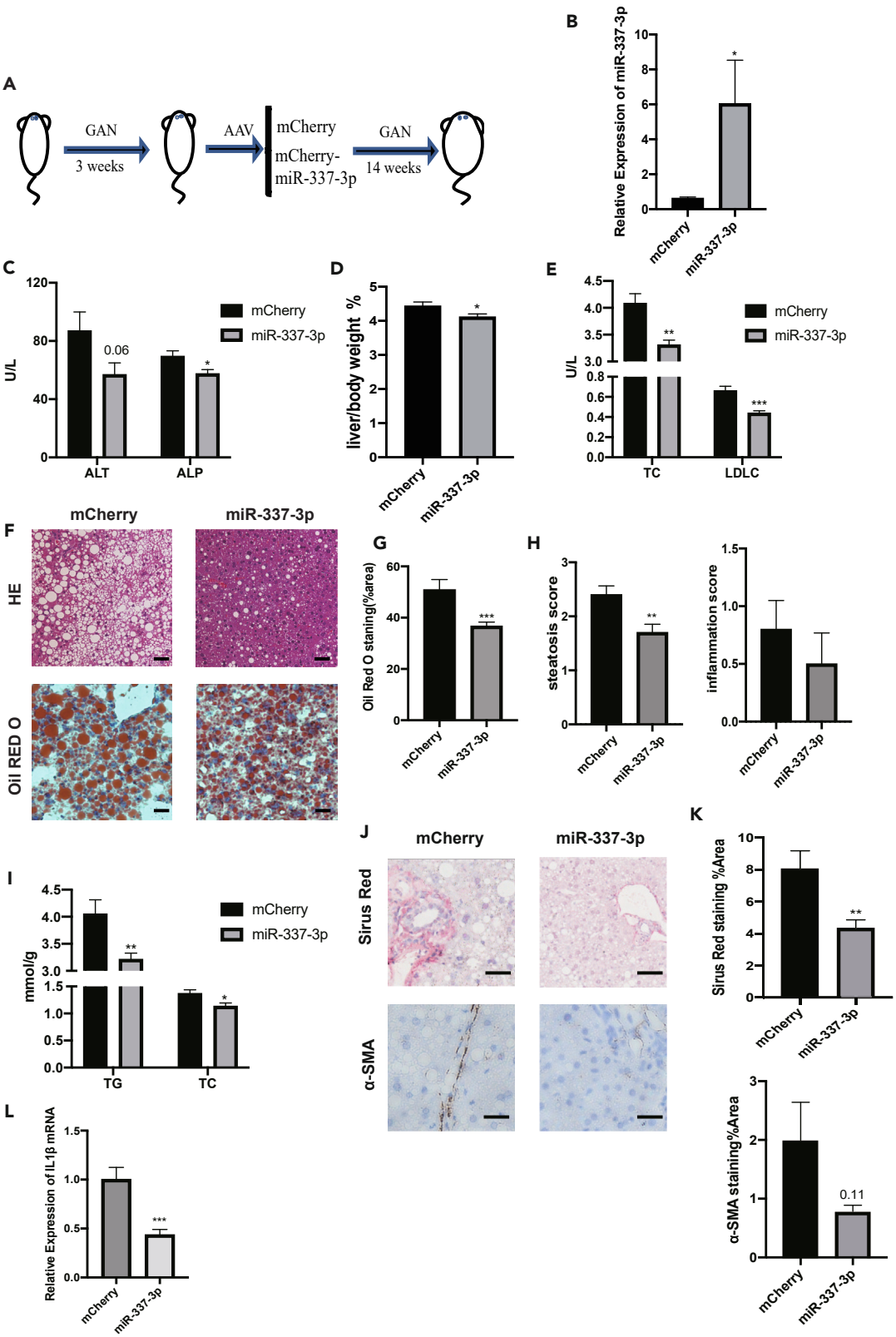
A
GAN
3 weeks
AAV
mCherry
mCherry-
miR-337-3p
GAN
14 weeks
B
Relative Expression of miR-337-3p
mCherry
miR-337-3p
C
U/L
mCherry
miR-337-3p
0.06
ALT
ALP
D
liver/body weight %
E
U/L
TC
LDLC
F
mCherry
miR-337-3p
HE
Oil RED O
G
Oil Red O staining(%area)
H
steatosis score
inflammation score
I
mmol/g
TG
TC
J
Sirus Red
α-SMA
K
Sirus Red staining %Area
α-SMA staining%Area
0.11
L
Relative Expression of IL1β mRNA

Figure 2. MiR-337-3p could ameliorate hepatic steatosis, inflammation, and fibrosis in GAN diet-induced mouse model

(A) The schematic diagram of GAN diet-induced mouse model.
(B) RT-qPCR analysis of the relative miR-337-3p levels in the miR-337-3p and mCherry groups.
(C) The contents of ALT and ALP in miR-337-3p and mCherry groups.
(D) The index of liver/body weight in miR-337-3p and mCherry groups.
(E) The contents of serum TC, LDL-C in miR-337-3p and mCherry groups.
(F) Representative H&E staining and oil red O staining of miR-337-3p and mCherry groups. Scale bar, 100 μm.
(G) Quantification of the area of oil red O staining of two groups.
(H) The scores of steatosis and inflammation of two groups.
(I) The relative levels of TG and TC in the livers of two groups.
(J) Representative Sirius red staining and immunohistochemical staining of α-SMA. Scale bar, 100 μm.
(K) Quantification of the area of Sirius red staining and immunohistochemical staining of α-SMA of two groups.
(L) RT-qPCR analysis of IL1β mRNA in miR-337-3p and mCherry groups. n = 10/each group. All results are presented as mean ± SEM. *$p < 0.05$, **$p < 0.01$, ***$p < 0.001$ versus the mCherry group.

GAN diet-induced mouse model[21,22](Figures 2A and S1). After 14 weeks of tail-vein injection of virus, the level of hepatic miR-337-3p was obviously increased (Figure 2B). Meanwhile, serum ALT and alkaline phosphatase levels and hepatosomatic index (the ratio of liver weight to body weight) of mice with miR-337-3p overexpression were lower than those of mice in the mCherry group obviously (Figures 2C and 2D), which indicated that miR-337-3p played a protective role in liver injury induced by overnutrition.

Next, we focused on the relevant indicators of lipid metabolism in this model. Consistent with our previous results,[20] miR-337-3p overexpression could improve dyslipidemia, where serum total cholesterol (TC) and LDL-C of miR-337-3p group were decreased obviously (Figure 2E). For the changes of liver fat content, H&E and oil red O staining of the liver sections were conducted. As shown in Figures 2F–2H, the miR-337-3p group had less macrovesicular steatosis and inflammation, as reflected by the lower histological scores according to pathophysiological evaluations, and mild accumulation of TG according to the results of oil red O staining and quantification. Furthermore, the hepatic TG and TC levels were reduced in miR-337-3p group when compared with mCherry group (Figure 2I), confirming again that miR-337-3p can regulate the lipid metabolism in the liver.

Since inflammation and fibrosis also are the pathological changes in NAFLD,[23] we further examined the effects of miR-337-3p on inflammation and fibrosis by staining the liver section with Sirius red and the immunohistochemical antibodies of α-SMA, Ly6G, and F4/80. Although the immunohistochemical staining of Ly6G and F4/80 did not make any difference between two groups (Figure S2), the miR-337-3p group had a lower score of inflammation (Figure 2H). Moreover, miR-337-3p could decrease the mRNA of IL1β (Figure 2L). Therefore, we inferred that miR-337-3p might alleviate inflammation by influencing other inflammatory cytokines, like IL1β. As shown in Figures 2J and 2K, miR-337-3p could reduce Sirius red and α-SMA staining area, which suggested it can attenuate the fibrosis of NAFLD.

Overexpression of miR-337-3p improved glucose metabolism in GAN diet- and HFD/STZ-induced mice

In the course of determining the effect of miR-337-3p on lipid metabolism disorder in GAN diet-induced mice, we also examined whether miR-337-3p affected the glucose metabolism in this mouse model. As shown in Figure 3A, serum fructosamine of mice with miR-337-3p overexpression was lower than that of the mCherry group. Moreover, the results of oral glucose tolerance test and HOMA-IR also indicated that miR-337-3p could relieve insulin resistance and ameliorate glucose metabolism disorder (Figures 3B and 3C). To further confirm the role of miR-337-3p in improving glucose metabolism, a type 2 diabetes mouse model induced by a high-fat diet (HFD) combined with streptozotocin (STZ) was used.[24,25] After tail-vein injection of the virus, the mice were fed with HFD for 40 days and then intraperitoneally injected with STZ, which led to the gradual increase in fasting blood glucose (FBG) in mCherry group, whereas FBG in miR-337-3p group increased slowly (Figures 3D–3F). With the extension of time, the increase of FBG caused by STZ injection in mCherry group recovered sluggishly, but once STZ was injected again, their FBG levels increased again. In other words, FBG levels in mCherry group elevated with the stimulation of STZ, which did not occur in miR-337-3p group. Subsequently, we also found that miR-337-3p could inhibit gluconeogenesis as determined by pyruvate tolerance test (Figure 3G) and increase glycogen content as illustrated by PAS staining and quantification (Figure 3H). Additionally, the effect of miR-337-3p on gluconeogenesis was verified using hepatocyte glucose production assay in primary hepatocytes from healthy mouse. Compared to negative control (NC), the primary hepatocytes transfected with miR-337-3p produced less glucose when stimulated by gluconeogenic substrates (Figure 3I).

Based on these results, miR-337-3p could improve glucose homeostasis in both GAN diet- and HFD/STZ-induced mouse models.

MiR-337-3p inhibited TG accumulation and relieved lipotoxicity *in vitro*

After discovering the benefit of miR-337-3p in improving hepatic lipid disorders, we detected related pathological characteristics in PA or FFA-stimulated HepG2 and L02 cells in the presence or absence of miR-337-3p. As shown in Figures 4A and 4B, the intracellular lipid accumulation induced by FFA was measured by oil red O staining, and it was apparent that the lipid droplets in the cells transfected with miR-337-3p were reduced. Similarly, the increase in intracellular TG content stimulated by FFA also decreased accordingly in miR-337-3p group (Figure 4C).

Since the lipid accumulation in cells also could lead to mitochondrial damage and a decline in cell viability,[26] we further examined the mitochondrial copy number, a surrogate marker for mitochondrial function,[27] and cell viability in PA-stimulated L02 cells. The results of

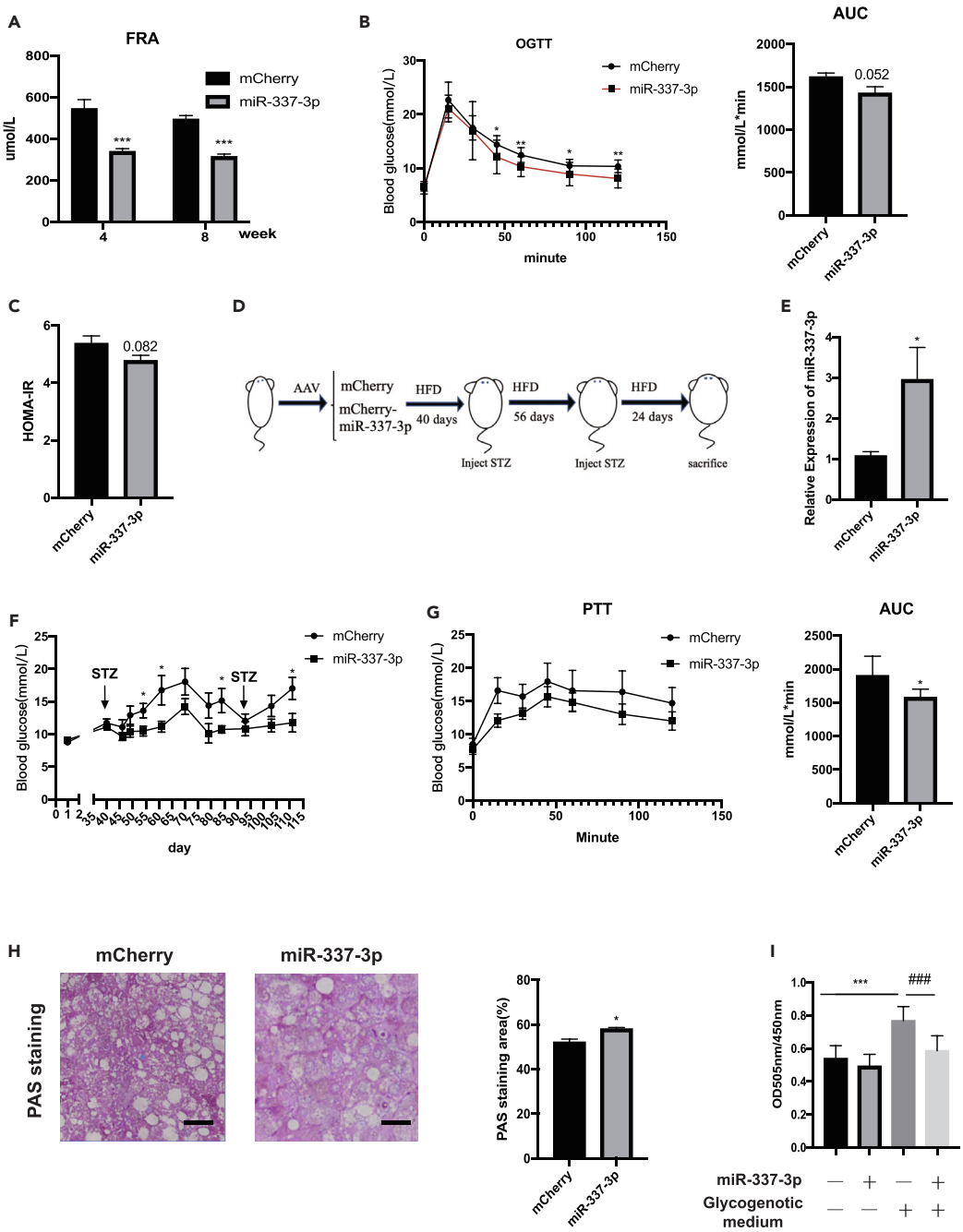

Figure 3. MiR-337-3p could regulate glucose metabolism in GAN diet and HFD/STZ-induced mouse model

(A) The content of FRA in the serum of miR-337-3p and mCherry groups (n = 10/each group) in GAN diet-induced mouse model at 4 and 8 weeks.

(B) The OGTT assay of miR-337-3p and mCherry groups (n = 10/each group).

(C) The index of HOMA-IR of miR-337-3p and mCherry groups (n = 10/each group).

(D) The schematic diagram of HFD/STZ mouse model.

(E) RT-qPCR analysis of the relative miR-337-3p levels in miR-337-3p and mCherry groups (n = 8/each group).

(F) The fasting blood glucose of miR-337-3p and mCherry groups (n = 8/each group).

(G) The PTT assay of miR-337-3p and mCherry groups (n = 8/each group).

(H) Representative PAS staining of miR-337-3p and mCherry groups and their quantification. Scale bar, 100 μm.

(I) The glucose output of primary hepatocyte transfected with NC or miR-337-3p. The results of A–H are presented as mean ± SEM. The results of I are presented as mean ± SD. *p < 0.05, **p < 0.01, ***p < 0.001 versus the mCherry or the control group. ###p < 0.001 versus the glycogenotic medium group without miR-337-3p in I.

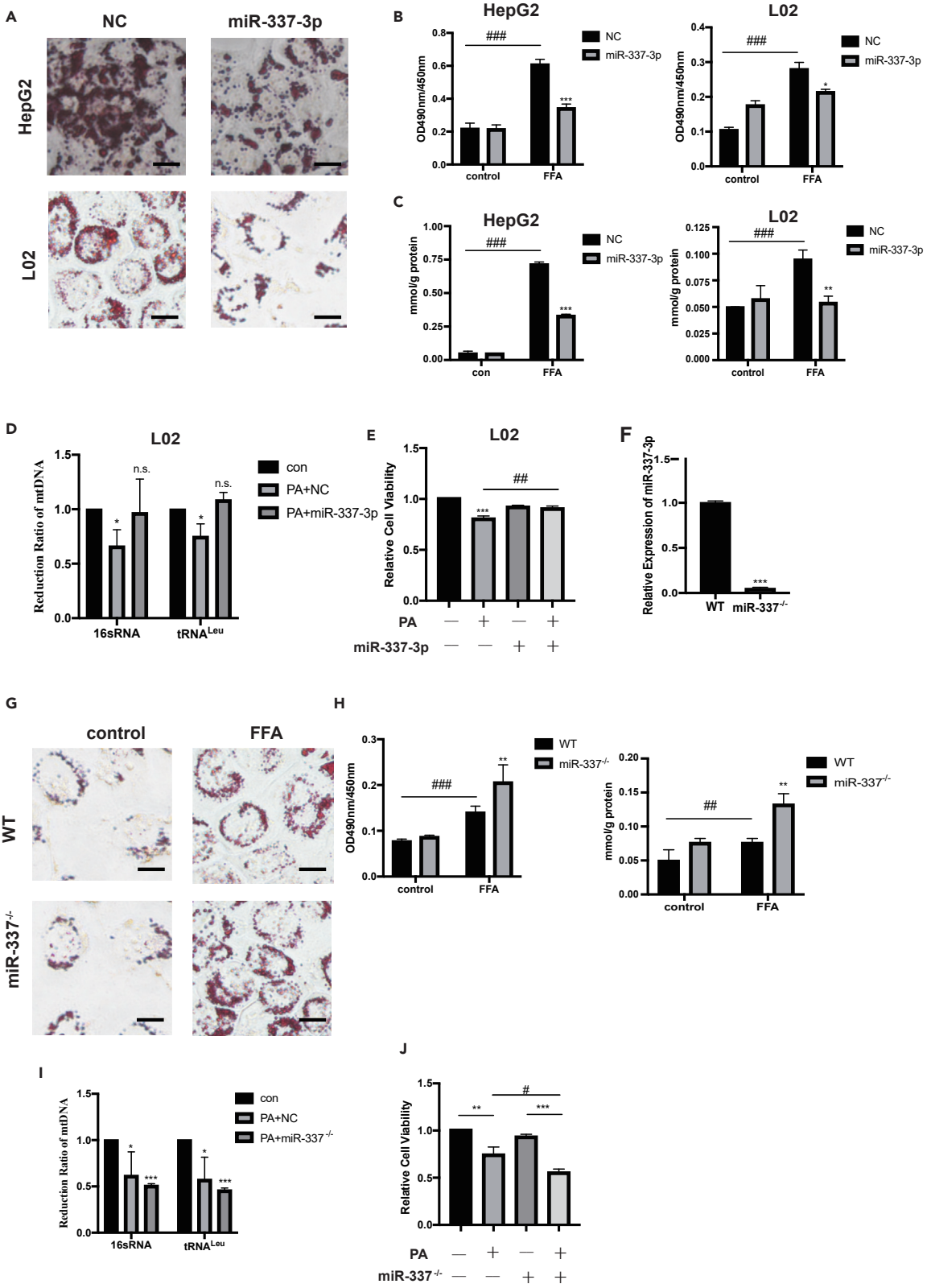
A
NC
miR-337-3p
HepG2
L02
B
HepG2
L02
NC
miR-337-3p
OD490nm/450nm
###
control
FFA
C
HepG2
L02
mmol/g protein
con
D
L02
Reduction Ratio of mtDNA
n.s.
16sRNA
tRNA^Leu
con
PA+NC
PA+miR-337-3p
E
L02
Relative Cell Viability
##
PA
miR-337-3p
F
Relative Expression of miR-337-3p
WT
miR-337-/-
G
control
FFA
WT
miR-337-/-
H
WT
miR-337-/-
I
PA+miR-337-/-
J
Relative Cell Viability
#

Figure 4. MiR-337-3p relieved the accumulation of lipid and lipotoxicity in cells

(A) Representative images of oil red O staining of HepG2 and L02 cells induced by FFA when transfected with NC or miR-337-3p. Scale bar = 20 μm.
(B) Quantification of oil red O staining in A.
(C) The contents of TG in HepG2 and L02 cells induced by FFA when transfected with NC or miR-337-3p.
(D) RT-qPCR analysis of mtDNA in L02 induced by PA in presence of NC or miR-337-3p.
(E) CCK8 analysis of relative cell viability in HepG2 induced by PA in presence of NC or miR-337-3p.
(F) Relative endogenous miR-337-3p levels in the WT and miR-337-3p knockout (miR-337$^{-/-}$) L02 cells via RT-qPCR analysis.
(G) Representative images of oil red O staining of the WT and miR-337$^{-/-}$ cells. Scale bar, 20 μm.
(H) Quantification of oil red O staining and TG in WT and miR-337$^{-/-}$ cells induced by FFA.
(I) RT-qPCR analysis of mtDNA in WT and miR-337$^{-/-}$ cells induced by PA.
(J) CCK8 analysis of relative cell viability in WT and miR-337$^{-/-}$ cells induced by PA. All results are presented as mean ± SD. *p < 0.05, **p < 0.01, ***p < 0.001 versus the NC group. #p < 0.05, ##p < 0.01, ###p < 0.001 versus the control group with NC in B, C, H and versus the PA group with NC in E, J.

Figures 4D and 4E demonstrated that miR-337-3p could blunt PA-induced decrease of mtDNA/nuclear DNA ratio and cell viability. Recently, that the metabolic dysregulation can induce cellular senescence is universally acknowledged.[28] Given miR-337-3p could recover the damaged mtDNA, one of hallmarkers of cellular senescence, we detected other senescence indicators, cleaved PARP and caspase-3, to further confirm its effect on cellular senescence. As shown in Figure S3, miR-337-3p could inhibit the increase of cleaved PARP and caspase-3 induced by PA treatment.

Considering the protective effects of exogenous miR-337-3p on lipotoxicity, we investigated whether endogenous miR-337-3p also played the same role. CRISPR-Cas9 was used to delete the genomic sequence of pre-miR-337, which led endogenous miR-337-3p to reduce drastically (Figure 4F). As shown in Figures 4G–4H, the lipid accumulation was more evident in the cells without miR-337-3p. Furthermore, the mitochondrial damage and cell viability of miR-337$^{-/-}$ were more significant or severe than wild type, too (Figures 4I and 4J).

MiR-337-3p might target multiple genes of glucose and lipid metabolism simultaneously

In view of the improved role of miR-337-3p in lipid accumulation, glucose homeostasis, mitochondrial disorder, and hepatocyte apoptosis, we were curious about its possible molecular mechanism. Firstly, differently expressed proteins between miR-337-3p-transfected and NC-transfected HepG2 cells were detected by mass spectrometry (MS). Compared to the NC, there were 788 downregulated proteins (FC < 0.083, p < 0.05) and 735 upregulated proteins (FC > 1.2, p < 0.05) (Figure 5A). Since the general pattern of miRNA regulating genes is to degrade mRNA or inhibit protein translation, we further focused on downregulated proteins. After KEGG pathway analysis (https://david.ncifcrf.gov/), 14.67% genes were mapped to metabolic pathway (Figure 5B). Moreover, the analysis of these downregulated genes via GSEA database (https://www.gsea-msigdb.org/gsea/index.jsp) revealed that fatty acid metabolism, cholesterol homeostasis, and cellular glucose homeostasis were the main enriched pathways (Figure 5C), which might contribute to the effects of miR-337-3p on improving glucose and lipid metabolism *in vivo* and *in vitro*. To verify the results of MS, we detected several key genes that play crucial roles in glycolipid metabolism (*FOXO1*/*Foxo1*, *G6PC*/*G6pc*, *PCK1*/*Pck1*, *SCD*/*Scd*, *FASN*/*Fasn*, *FABP1*/*Fabp1*, *HMGCR*/*Hmgcr*) in miR-337-3p-transfected HepG2 cells (Figure 5D) and primary hepatocytes from healthy mouse (Figure 5E), the liver tissues from miR-337-3p-overexpressed mice (Figure 5F), and miR-337-3p knockout cells (Figure 5G). The results indicated that the genes identified by MS (*FOXO1*, *SCD*, *FASN*, *FABP1*, *HMGCR*) and the related downstream genes (*G6PC*, *PCK1*) were decreased under the condition of overexpressing miR-337-3p *in vitro* and *in vivo* (Figures 5D–5F, Table 1). On the contrary, those genes were increased significantly when the endogenous miR-337-3p expression was lower (Figure 5G). Moreover, the reduction of these genes at protein and mRNA levels were also observed in miR-337-3p-transfected primary hepatocytes from healthy mouse when stimulated with FFA or not (Figures S4A–S4C), which suggested that miR-337-3p could regulate multiple glycolipid metabolism-associated genes in the *in vitro* NAFLD model. Furthermore, its inhibitory effects on gluconeogenesis and TG accumulation was also verified in this model through detecting glucose production stimulated by gluconeogenic substrates (Figure S4D), the staining of oil red O (Figure S4E), and the level of TG (Figure S4F).

Finally, we analyzed the relationship between miR-337 and 7 genes separately (Figure S5) in GSE89632, in which miR-337 negatively correlated with *SCD*, *FASN*, *FABP1*, and *HMGCR* (Figures S5A–S5D), whereas it was not associated with *FOXO1*, *G6PC*, and *PCK1* (data not shown). We speculated that the data of NAFL/NASH patients without diabetes might affect the result, and when we only analyzed the data of healthy controls and diabetic patients in this database, the negative correlation between *miR-337* and *PCK1* can be obtained (Figure S5E).

Taken together, we speculated that miR-337-3p might regulate multiple genes involved in glucose and lipid metabolism simultaneously to exert beneficial effects on glycolipid metabolism disorders.

A validation example: HMGCR is the target of miR-337-3p

Since miR-337-3p can regulate multiple genes simultaneously to play regulatory roles, we would select a representative gene for further verification. Firstly, BioCyc (https://BioCyc.org), a database of metabolic reactions and enzymes,[29] was used to analyze 109 genes in metabolic pathway from Figure 5B, where cholesterol biosynthesis is the most relevant pathway (Figure 6A). Within those genes, we chose HMGCR, a key protein in cholesterol homeostasis, to verify that it could be influenced by miR-337-3p directly. Next, we examined the protein levels of HMGCR in HepG2 cells and GAN-diet induced mice with miR-337-3p overexpression. Compared with the respective control group, the protein contents of HMGCR were downregulated with miR-337-3p overexpression (Figures 6B and 6C), which was consistent with the results of MS. As expected, the mRNA of HMGCR was reduced dependently on miR-337-3p concentration gradient (Figure 6D).

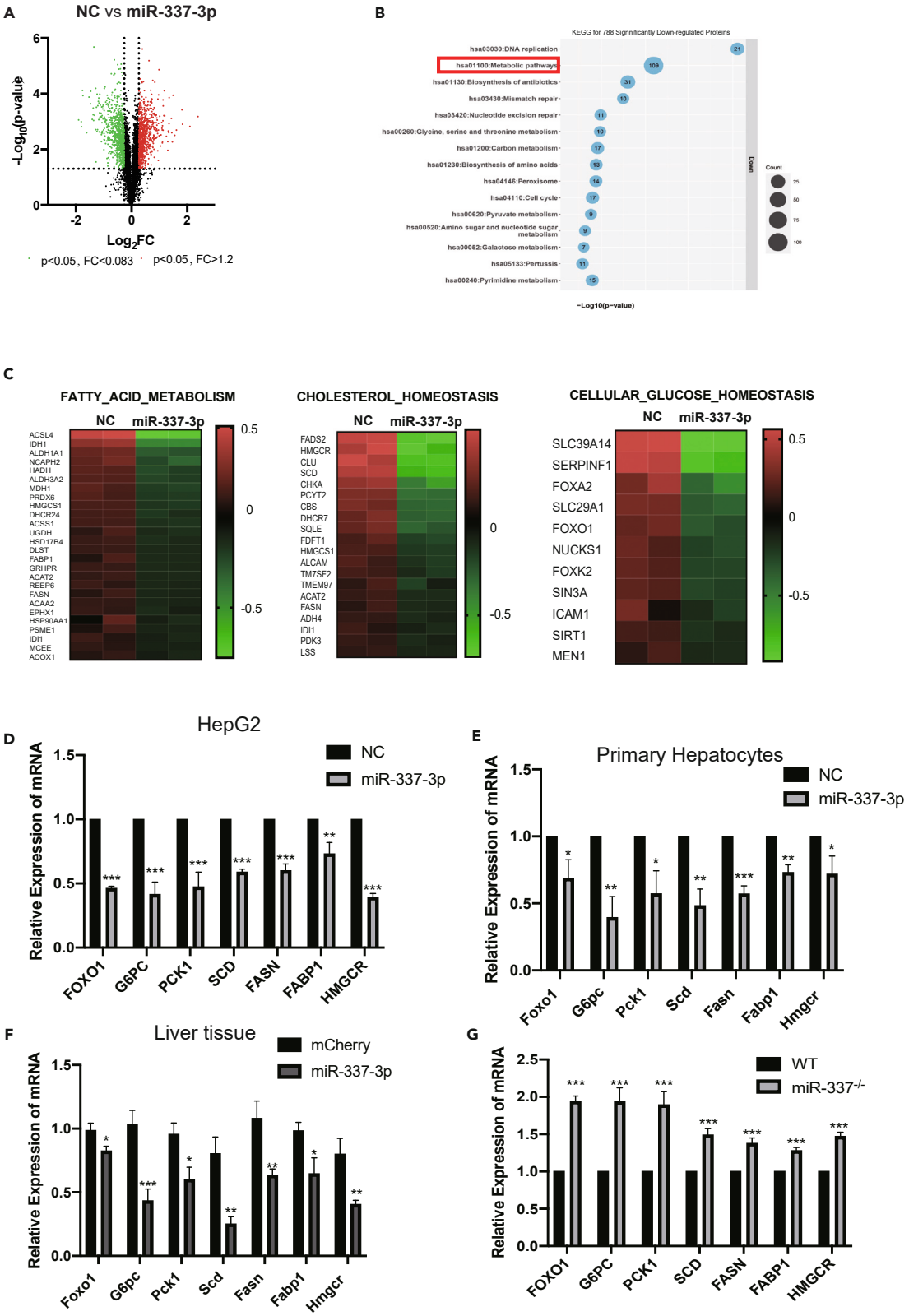
A
NC vs miR-337-3p
-Log10(p-value)
Log2FC
p<0.05, FC<0.083
p<0.05, FC>1.2
B
KEGG for 788 Signnificantly Down-regulated Proteins
hsa03030:DNA replication
hsa01100:Metabolic pathways
hsa01130:Biosynthesis of antibiotics
hsa03430:Mismatch repair
hsa03420:Nucleotide excision repair
hsa00260:Glycine, serine and threonine metabolism
hsa01200:Carbon metabolism
hsa01230:Biosynthesis of amino acids
hsa04146:Peroxisome
hsa04110:Cell cycle
hsa00620:Pyruvate metabolism
hsa00520:Amino sugar and nucleotide sugar metabolism
hsa00052:Galactose metabolism
hsa05133:Pertussis
hsa00240:Pyrimidine metabolism
Down
Count
-Log10(p-value)
C
FATTY_ACID_METABOLISM
CHOLESTEROL_HOMEOSTASIS
CELLULAR_GLUCOSE_HOMEOSTASIS
NC
miR-337-3p
ACSL4
IDH1
ALDH1A1
NCAPH2
HADH
ALDH3A2
MDH1
PRDX6
HMGCS1
DHCR24
ACSS1
UGDH
HSD17B4
DLST
FABP1
GRHPR
ACAT2
REEP6
FASN
ACAA2
EPHX1
HSP90AA1
PSME1
IDI1
MCEE
ACOX1
FADS2
HMGCR
CLU
SCD
CHKA
PCYT2
CBS
DHCR7
SQLE
FDFT1
HMGCS1
ALCAM
TM7SF2
TMEM97
ACAT2
FASN
ADH4
IDI1
PDK3
LSS
SLC39A14
SERPINF1
FOXA2
SLC29A1
FOXO1
NUCKS1
FOXK2
SIN3A
ICAM1
SIRT1
MEN1
D
HepG2
NC
miR-337-3p
Relative Expression of mRNA
FOXO1
G6PC
PCK1
SCD
FASN
FABP1
HMGCR
E
Primary Hepatocytes
Foxo1
G6pc
Pck1
Scd
Fasn
Fabp1
Hmgcr
F
Liver tissue
mCherry
G
WT
miR-337-/-

Figure 5. Searching the possible target of miR-337-3p by MS

(A) Volcano plot of differentially expressed proteins detected by MS in HepG2 cells which were overexpressed miR-337-3p versus NC (n = 2/each group).

(B) KEGG pathway enrichment bubble chart of differentially expressed proteins.

(C) Pathway enrichment analysis by GSEA.

(D–G) The mRNA levels of *FOXO1*/*Foxo1*, *G6PC*/*G6pc*, *PCK1*/*Pck1*, *SCD*/*Scd*, *FASN*/*Fasn*, *FABP1*/*Fabp1*, and *HMGCR*/*Hmgcr* in HepG2 (D) and primary hepatocytes from healthy mice(E) transfected with or without miR-337-3p (30 nM), in the livers of miRNA overexpressed or control mice which induced by GAN diet (n = 10/each group) (F), and in WT or miR-337$^{-/-}$ cells (G). The results of D, E, and G are presented as mean ± SD. The results of F are presented as mean ± SEM. *p < 0.05, **p < 0.01, ***p < 0.001 versus the NC, mCherry, or WT group.

After confirming the effects of miR-337-3p on HMGCR mRNA and protein levels, related molecular mechanism was investigated. Because the classical mode of miRNA-regulating gene is to bind to the 3′UTR region of the target gene,[6,30] we constructed the luciferase reporter plasmid of *HMGCR* 3′UTR. As illustrated in Figure 6E, miR-337-3p suppressed luciferase activity dose dependently. According to the principle of complementary base pairing, there is a seven-base sequence in miR-337-3p matching with 3′UTR of *HMGCR* (Figure S6A). When we mutated this sequence, miR-337-3p-MUT failed to inhibit *HMGCR* (Figure S6B and S6C).

It has been reported that lipotoxicity can damage mitochondrial function, promote c-Jun N-terminal kinases (JNK) activation, and induce cell apoptosis, which can be abolished by lowering of free cholesterol.[31] Since HMGCR controls the rate-limiting step in the cholesterol biosynthetic pathway,[32] we also tested the activities of miR-337-3p in regulating the PA-stimulated increase of JNK phosphorylation and decrease of cell viability. The results from Figures 6F and 6G demonstrated that miR-337-3p could inhibit the phosphorylation of JNK and recover the viability of cells induced by PA treatment, which was disappeared when HMGCR was overexpressed (Figures 6F and 6G). Furthermore, miR-337$^{-/-}$ cells showed more obvious increase in JNK phosphorylation and decrease in cell viability under PA stimulation, and this phenomenon also did not occur after HMGCR was knocked down (Figures 6H and 6I).

As a result, miR-337-3p could target HMGCR directly and alleviate lipotoxicity via HMGCR.

DISCUSSION

It is well known that the disorders of epigenetic processes can influence chromosomal stability and gene expression, resulting in complicated syndromes including obesity, MAFLD, diabetes, etc. miRNAs, as an important part of epigenetics, represent a class of transcriptional or post-transcriptional regulators of gene expression. Since the differentially expressed miRNAs during MAFLD may participate in the occurrence and development of this disease, it is necessary to clarify the biological functions of these miRNAs to understand the related pathogenesis. In the current study, we discovered that miR-337-3p is downregulated in SS and NASH patient and *in vivo*/*in vitro* experimental models, can ameliorate hepatic lipid accumulation, reduce fasting blood glucose, and improve insulin resistance via targeting multiple genes of glucose and lipid metabolism. These results indicated that the decrease of miR-337-3p might cause a series of glycolipid metabolism disorders, thereby helping the development or deterioration of the disease. Furthermore, we also discovered that miR-337-3p overexpression could remit liver inflammation and fibrosis reflected by the decrease of IL1β and smaller Sirius red-positive staining area, which suggested its potential in the treatment of NAFLD.

miRNAs typically regulate multiple targets, and a phenotype observed upon miRNA inhibition or overexpression is a composite result of regulation of several targets. Some miRNAs can repress multiple target mRNAs directly in one entire pathway or one phenotype, such as that miR-223 could protect against atherosclerosis via targeting SP3 and ABCA1[33] and miR-132-induced hepatic steatosis and hyperlipidemia via targeting FoxO3, Sirt1, and Pten.[9] Other miRNAs regulate target genes indirectly via targeting their transcription factors, for example, miR-552-3p could modulate transcriptional activities of FXR and LXRα to ameliorate hepatic glycolipid metabolism disorder[34] and miR-200 could regulate transcription factor ZEB1 during tumor metastasis.[35] In our work, some key genes regulating lipid metabolism (*SCD*, *FASN*, *FABP1*, *HMGCR*, etc.) might be mediated directly by miR-337-3p, because possible binding sites of miR-337-3p on their 3′UTR can be found through base complementary pairing principle (data not shown). While, miR-337-3p inhibited gluconeogenic genes (*G6PC*, *PCK1*) indirectly by regulating their transcription factors, *FOXO1*. Although we take the regulation of miR-337-3p on HMGCR as an example to prove its direct regulation on these genes, we still need further experimental verification for each gene. In addition, some gene knockout mice will be adopted to study the association between miR-337-3p improving NAFLD and its targets, such as HMGCR knockout mouse model.

As reported, liver is the major metabolic control hub to maintain energy and nutrient homeostasis, which makes it easy to become the target organ of metabolic syndrome. It is observed that MAFLD has high rates of diabetes mellitus (DM) (23%) and it is vice versa (MAFLD occurs very commonly in DM). Actually, DM and MAFLD usually coexist and would deteriorate related pathological features each other.[36] Therefore, it is beneficial to use one strategy to target both diseases simultaneously. We discovered that miR-337-3p could regulate glycolipid metabolism simultaneously, inhibit hepatic steatosis in GAN diet-induced mouse model, and suppress the increase of fasting blood glucose in HFD/STZ mouse model, suggesting that it might have broader application prospects.

It has been found that an altered epigenetic profile that is associated with the development of a disease state can be used as a biomarker in some cases, especially miRNAs in some glycolipid metabolic diseases, like type 2 diabetes mellitus (T2DM) and NAFLD. It has been reported that the expression of miR-146a and miR-223 is associated with T2DM.[37,38] Similarly, recent studies reported that miR-29, miR-1296, miR-132, and miR-135 were dysregulated in NAFL patients and correlated with the risk of disease onset.[39–43] Although miR-337-3p has different expression between patients and healthy people in some diseases, its content in blood under pathological condition of MAFLD is uncertain. In subsequent studies, more research is needed to confirm the potential of miR-337-3p as an MAFLD marker.

Table 1. The sequences of primers for real-time PCR

Species	Genes	Forward sequences (5′–3′)	Reverse sequences (5′–3′)
Human	GAPDH	GGAGCGAGATCCCTCCAAAAT	GGCTGTTGTCATACTTCTCATGG
	FOXO1	TCGTCATAATCTGTCCCTACACA	CGGCTTCGGCTCTTAGCAAA
	G6PC	GTGTCCGTGATCGCAGACC	GACGAGGTTGAGCCAGTCTC
	PCK1	AAAACGGCCTGAACCTCTCG	ACACAGCTCAGCGTTATTCTC
	SCD	TCTAGCTCCTATACCACCACCA	TCGTCTCCAACTTATCTCCTCC
	FASN	AAGGACCTGTCTAGGTTTGATGC	TGGCTTCATAGGTGACTTCCA
	FABP1	GTGTCGGAAATCGTGCAGAAT	GACTTTCTCCCCTGTCATTGTC
	HMGCR	TGATTGACCTTTCCAGAGCAAG	CTAAAATTGCCATTCCACGAGC
Mouse	Gapdh	AGGTCGGTGTGAACGGATTTG	GGGGTCGTTGATGGCAACA
	Foxo1	CCCAGGCCGGAGTTTAACC	GTTGCTCATAAAGTCGGTGCT
	G6pc	CGACTCGCTATCTCCAAGTGA	GGGCGTTGTCCAAACAGAAT
	Pck1	CTGCATAACGGTCTGGACTTC	GCCTTCCACGAACTTCCTCAC
	Scd	TTCTTGCGATACACTCTGGTGC	CGGGATTGAATGTTCTTGTCGT
	Fasn	GGAGGTGGTGATAGCCGGTAT	TGGGTAATCCATAGAGCCCAG
	Fabp1	ATGAACTTCTCCGGCAAGTACC	GGTCCTCGGGCAGACCTAT
	Hmgcr	AGCTTGCCCGAATTGTATGTG	TCTGTTGTGAACCATGTGACTTC

In conclusion, our study revealed the biological function of miR-337-3p in regulating glycolipid metabolism and proved that miR-337-3p could improve lipid and glucose metabolism by targeting multiple genes, indicating that miR-337-3p might be a novel therapeutic target for MAFLD in the future.

Limitations of the study

In the current study, we speculated that miR-337-3p could target multiple glycolipid metabolism-related genes, in which we took HMGCR as a validation example. However, which differentially expressed proteins obtained from MS are regulated directly by miR-337-3p awaits further investigation. In addition to verifying the interaction between miR-337-3p and the 3′UTRs of these genes, gene knockout mice should also be needed to prove the association between miR-337-3p improving NAFLD and its targets. When investigating the biological function of miR-337-3p, we detected the lipid accumulation and lipotoxicity in miR-337-3p-transfected or knockout cells and examined the phenotypes related to glycolipid metabolism in miR-337-3p-overexpressed mice. In order to gain a more comprehensive understanding of the function of miR-337-3p, its gene knockout mouse also should be considered in the future work. Additionally, we discovered that miR-337-3p could alleviate inflammation and fibrosis of the liver in GAN diet-induced mice, featured by lower histological scores of inflammation, decrease of IL1β mRNA, and reduced Sirius red and α-SMA staining area. Since the mouse fed with GAN diet for 17 weeks would not exhibited severe inflammation and fibrosis, the effect of miR-337-3p on inflammation and fibrosis should be confirmed in other mouse models and more indicators need to be detected, like some other inflammatory cytokines,[44] the level of HS-CRP,[45] etc.

STAR★METHODS

Detailed methods are provided in the online version of this paper and include the following:

- KEY RESOURCES TABLE
- RESOURCE AVAILABILITY
  - Lead contact
  - Materials availability
  - Data and code availability
- EXPERIMENTAL MODEL AND STUDY PARTICIPANT DETAILS
  - Cell lines
  - Animal experiments
- METHOD DETAILS
  - Adeno-associated virus construction
  - Oral glucose tolerance tests (OGTT) and pyruvate-tolerance test (PTT)
  - Primary mouse hepatocytes culture
  - Plasmids construction

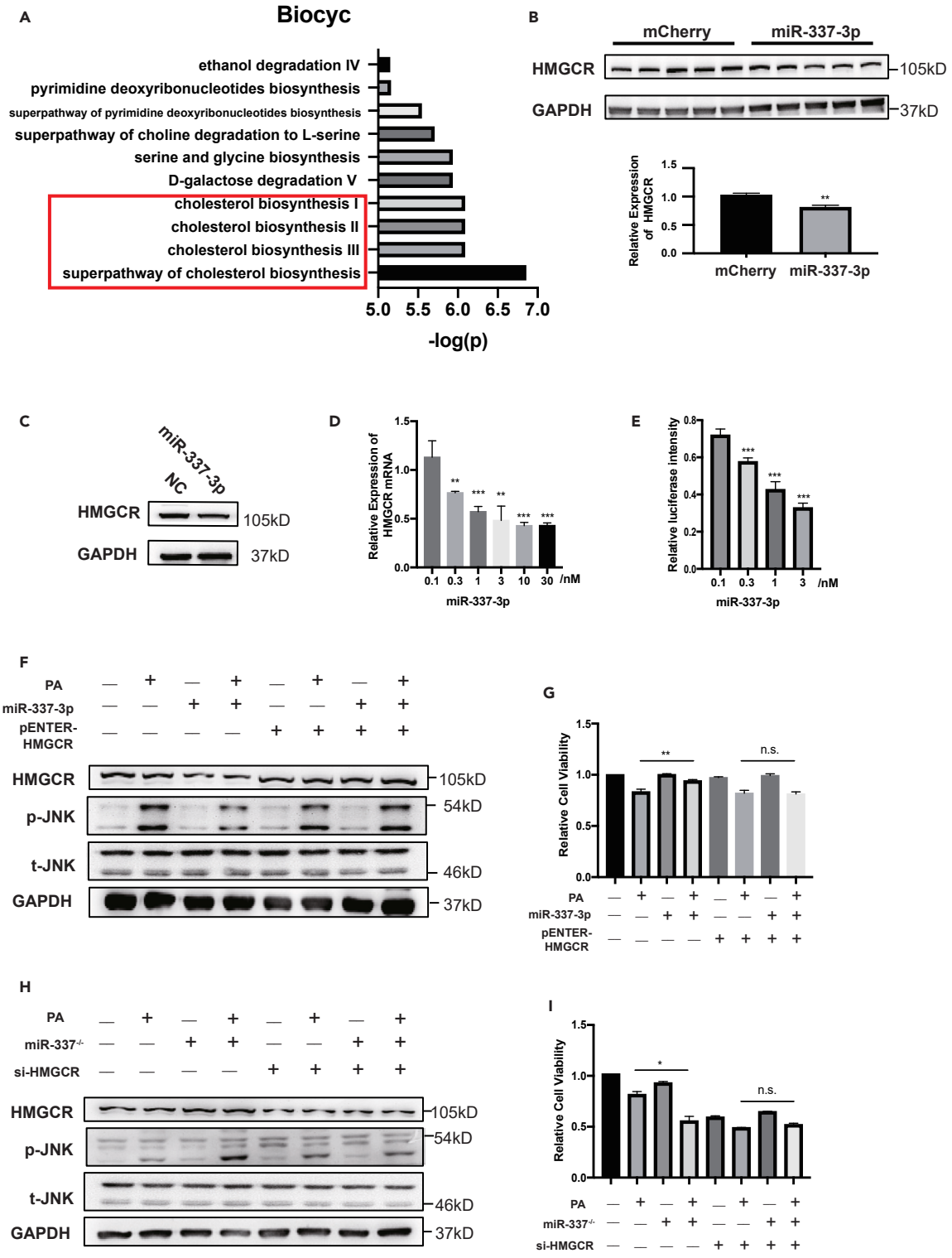

Figure 6. MiR-337-3p could target HMGCR/p-JNK pathway directly

(A) BioCyc analysis of differentially expressed proteins enriched in metabolic pathway.

(B) Western blot analysis of HMGCR proteins in the livers of miRNA overexpressed and control mice (n = 10/each group) and their quantification.

(C) Western blot analysis of HMGCR proteins in HepG2 cells after transfected with miR-337-3p (30 nM) or NC (30 nM).

(D) RT-qPCR analysis of *HMGCR* mRNA in HepG2 cells after transfected miR-337-3p or NC at different concentrations.

Figure 6. *Continued*

(E) The relative luciferase activities of *HMGCR* 3′UTR in HEK293 cells transfected with miR-337-3p at different concentrations.

(F) Western blot analysis of HMGCR, p-/t-JNK. HepG2 cells were transfected with miR-337-3p and penter-HMGCR for 48 h, and then incubated with or without PA for 8 h.

(G) CCK8 analysis of HepG2 cells which were transfected with miR-337-3p and penter-HMGCR for 48 h and incubated with or without PA for 8 h.

(H) Western blot analysis of HMGCR, p-/t-JNK. miR-337$^{-/-}$, or WT cells were transfected with siHMGCR for 48 h and incubated with or without PA for 8 h.

(I) CCK8 analysis of miR-337$^{-/-}$ or WT cells that were transfected with siHMGCR for 48 h and incubated with or without PA for 8 h. All results are presented as mean ± SD. *p < 0.05, **p < 0.01, ***p < 0.001 versus the control group.

- Luciferase assay
- Western blot analysis
- Real-time quantitative PCR analysis
- Staining of liver sections
- Biochemical analysis
- Mass spectrometry (MS)
- CRISPR/Cas9-mediated knockout of miR-337-3p

● QUANTIFICATION AND STATISTICAL ANALYSIS

SUPPLEMENTAL INFORMATION

Supplemental information can be found online at https://doi.org/10.1016/j.isci.2023.108352.

ACKNOWLEDGMENTS

We thank the Institutional Technology Service Center of Shanghai Institute of Materia Medica, Chinese Academy of Sciences for technical assistance in mass spectrometry experiments and analysis. This work was supported by Innovation Team and Talents Cultivation Program of National Administration of Traditional Chinese Medicine (No: ZYYCXTD-D-202210), Foundation of Shanghai Science and Technology Committee (Grant numbers: 21DZ2291100).

AUTHOR CONTRIBUTIONS

X.X., J.C., and J.R.: conceptualization; X.X., H.H., C.Y., X.P., and A.H.: investigation; R.T., L.G., and J.F.: methodology, software; X.X. and J.C.: writing – original draft preparation. All authors have made important suggestions regarding the manuscript.

DECLARATION OF INTERESTS

The authors declare no competing interests.

INCLUSION AND DIVERSITY

We support inclusive, diverse, and equitable conduct of research.

Received: May 17, 2023
Revised: July 26, 2023
Accepted: October 24, 2023
Published: October 28, 2023

REFERENCES

1. Tomic, D., Kemp, W.W., and Roberts, S.K. (2018). Nonalcoholic fatty liver disease: current concepts, epidemiology and management strategies. Eur. J. Gastroenterol. Hepatol. *30*, 1103–1115.
2. Dietrich, P., and Hellerbrand, C. (2014). Non-alcoholic fatty liver disease, obesity and the metabolic syndrome. Best Pract. Res. Clin. Gastroenterol. *28*, 637–653.
3. Fouad, Y., Palmer, M., Chen, M., Regev, A., Banerjee, R., Myers, R., Riccio, R., Torstenson, R., Younes, R., Arora, P.S., et al. (2022). Redefinition of Fatty Liver Disease from NAFLD to MAFLD through the Lens of Drug Development and Regulatory Science. J. Clin. Transl. Hepatol. *10*, 374–382.
4. Gjorgjieva, M., Sobolewski, C., Dolicka, D., Correia de Sousa, M., and Foti, M. (2019). miRNAs and NAFLD: from pathophysiology to therapy. Gut *68*, 2065–2079.
5. Ambros, V. (2004). The functions of animal microRNAs. Nature *431*, 350–355.
6. Bartel, D.P. (2009). MicroRNAs: target recognition and regulatory functions. Cell *136*, 215–233.
7. Filipowicz, W., Bhattacharyya, S.N., and Sonenberg, N. (2008). Mechanisms of post-transcriptional regulation by microRNAs: are the answers in sight? Genetics *9*, 102–114.
8. Rahbar, S., Pashaiasl, M., Ezzati, M., Ahmadi AsrBadr, Y., Mohammadi-Dehcheshmeh, M., Mohammadi, S.A., and Ghaffari Novin, M. (2020). MicroRNA-based regulatory circuit involved in sperm infertility. Andrologia *52*, e13453.
9. Hanin, G., Yayon, N., Tzur, Y., Haviv, R., Bennett, E.R., Udi, S., Krishnamoorthy, Y.R., Kotsiliti, E., Zangen, R., Efron, B., et al. (2018). miRNA-132 induces hepatic steatosis and hyperlipidaemia by synergistic multitarget suppression. Gut *67*, 1124–1134.
10. Su, Q., Kumar, V., Sud, N., and Mahato, R.I. (2018). MicroRNAs in the pathogenesis and treatment of progressive liver injury in NAFLD and liver fibrosis. Adv. Drug Deliv. Rev. *129*, 54–63.
11. Xiao, W., Yao, E., Zheng, W., Tian, F., and Tian, L. (2017). miR-337 can be a key negative regulator in melanoma. Cancer Biol. Ther. *18*, 392–399.

12. Xiang, X., Mei, H., Zhao, X., Pu, J., Li, D., Qu, H., Jiao, W., Zhao, J., Huang, K., Zheng, L., and Tong, Q. (2015). miRNA-337-3p suppresses neuroblastoma progression by repressing the transcription of matrix metalloproteinase 14. Oncotarget *6*, 22452–22466.
13. Kim, S.Y., Lee, Y.H., and Bae, Y.S. (2012). MiR-186, miR-216b, miR-337-3p, and miR-760 cooperatively induce cellular senescence by targeting alpha subunit of protein kinase CKII in human colorectal cancer cells. Biochem. Biophys. Res. Commun. *429*, 173–179.
14. Li, Q., Huang, Q., Cheng, S., Wu, S., Sang, H., and Hou, J. (2019). Circ_ZNF124 promotes non-small cell lung cancer progression by abolishing miR-337-3p mediated downregulation of JAK2/STAT3 signaling pathway. Cancer Cell Int. *19*, 291.
15. Zhou, X.Y., Yang, H., Bai, Y.Q., Li, X.L., Han, S.Y., and Zhou, B.X. (2020). hsa_circ_0006916 promotes hepatocellular carcinoma progression by activating the miR-337-3p/STAT3 axis. Cell. Mol. Biol. Lett. *25*, 47.
16. Wang, Z., Yao, L., Li, Y., Hao, B., Wang, M., Wang, J., Gu, W., Zhan, H., Liu, G., and Wu, Q. (2020). miR-337-3p inhibits gastric tumor metastasis by targeting ARHGAP10. Mol. Med. Rep. *21*, 705–719.
17. Pan, Y., Zhao, Y., Lihui, L., Xie, Y., and Zou, Q. (2021). MiR-337-3p suppresses migration and invasion of breast cancer cells by downregulating ESRP1. Acta Histochem. *123*, 151777.
18. Jian, S., Luo, D., Wang, Y., Xu, W., Zhang, H., Zhang, L., and Zhou, X. (2023). MiR-337-3p confers protective effect on facet joint osteoarthritis by targeting SKP2 to inhibit DUSP1 ubiquitination and inactivate MAPK pathway. Cell Biol. Toxicol. *39*, 1099–1118.
19. Demarez, C., Gérard, C., Cordi, S., Poncy, A., Achouri, Y., Dauguet, N., Rosa, D.A., Gunning, P.T., Manfroid, I., and Lemaigre, F.P. (2018). MicroRNA-337-3p controls hepatobiliary gene expression and transcriptional dynamics during hepatic cell differentiation. Hepatology *67*, 313–327.
20. Xu, X., Dong, Y., Ma, N., Kong, W., Yu, C., Gong, L., Chen, J., and Ren, J. (2021). MiR-337-3p lowers serum LDL-C level through targeting PCSK9 in hyperlipidemic mice. Metabolism *119*, 154768.
21. Song, Y., Wei, J., Li, R., Fu, R., Han, P., Wang, H., Zhang, G., Li, S., Chen, S., Liu, Z., et al. (2023). Tyrosine kinase receptor B attenuates liver fibrosis by inhibiting TGF-β/SMAD signaling. Hepatology *78*, 1433–1447.
22. Lewis, L.C., Chen, L., Hameed, L.S., Kitchen, R.R., Maroteau, C., Nagarajan, S.R., Norlin, J., Daly, C.E., Szczerbinska, I., Hjuler, S.T., et al. (2023). Hepatocyte mARC1 promotes fatty liver disease. JHEP Rep. *5*, 100693.
23. Ajmera, V., and Loomba, R. (2021). Imaging biomarkers of NAFLD, NASH, and fibrosis. Mol. Metabol. *50*, 101167.
24. Srinivasan, K., Viswanad, B., Asrat, L., Kaul, C.L., and Ramarao, P. (2005). Combination of high-fat diet-fed and low-dose streptozotocin-treated rat: a model for type 2 diabetes and pharmacological screening. Pharmacol. Res. *52*, 313–320.
25. Cassano, V., Leo, A., Tallarico, M., Nesci, V., Cimellaro, A., Fiorentino, T.V., Citraro, R., Hribal, M.L., De Sarro, G., Perticone, F., et al. (2020). Metabolic and Cognitive Effects of Ranolazine in Type 2 Diabetes Mellitus: Data from an *in vivo* Model. Nutrients *12*, 382.
26. Ipsen, D.H., Lykkesfeldt, J., and Tveden-Nyborg, P. (2018). Molecular mechanisms of hepatic lipid accumulation in non-alcoholic fatty liver disease. Cell. Mol. Life Sci. *75*, 3313–3327.
27. Venegas, V., and Halberg, M.C. (2012). Measurement of mitochondrial DNA copy number. Methods Mol. Biol. *837*, 327–335.
28. Meijnikman, A.S., Herrema, H., Scheithauer, T.P.M., Kroon, J., Nieuwdorp, M., and Groen, A.K. (2021). Evaluating causality of cellular senescence in non-alcoholic fatty liver disease. JHEP Rep. *3*, 100301.
29. Paley, S., and Karp, P.D. (2021). The BioCyc Metabolic Network Explorer. BMC Bioinf. *22*, 208.
30. Lewis, B.P., Burge, C.B., and Bartel, D.P. (2005). Conserved seed pairing, often flanked by adenosines, indicates that thousands of human genes are microRNA targets. Cell *120*, 15–20.
31. Van Rooyen, D.M., Gan, L.T., Yeh, M.M., Haigh, W.G., Larter, C.Z., Ioannou, G., Teoh, N.C., and Farrell, G.C. (2013). Pharmacological cholesterol lowering reverses fibrotic NASH in obese, diabetic mice with metabolic syndrome. J. Hepatol. *59*, 144–152.
32. Lu, X.Y., Shi, X.J., Hu, A., Wang, J.Q., Ding, Y., Jiang, W., Sun, M., Zhao, X., Luo, J., Qi, W., and Song, B.L. (2020). Feeding induces cholesterol biosynthesis via the mTORC1-USP20-HMGCR axis. Nature *588*, 479–484.
33. Nguyen, M.A., Hoang, H.D., Rasheed, A., Duchez, A.C., Wyatt, H., Cottee, M.L., Graber, T.E., Susser, L., Robichaud, S., Berber, İ., et al. (2022). miR-223 Exerts Translational Control of Proatherogenic Genes in Macrophages. Circ. Res. *131*, 42–58.
34. Fan, L., Lai, R., Ma, N., Dong, Y., Li, Y., Wu, Q., Qiao, J., Lu, H., Gong, L., Tao, Z., et al. (2021). miR-552-3p modulates transcriptional activities of FXR and LXR to ameliorate hepatic glycolipid metabolism disorder. J. Hepatol. *74*, 8–19.
35. Reshmi, G., Sona, C., and Pillai, M.R. (2011). Comprehensive patterns in microRNA regulation of transcription factors during tumor metastasis. J. Cell. Biochem. *112*, 2210–2217.
36. Lee, W.L., Wang, P.H., Yang, S.T., Liu, C.H., Chang, W.H., and Lee, F.K. (2022). To do one and to get more: Part II. Diabetes and metabolic dysfunction-associated fatty liver diseases. J. Chin. Med. Assoc. *85*, 1109–1119.
37. Alipoor, B., Ghaedi, H., Meshkani, R., Torkamandi, S., Saffari, S., Iranpour, M., and Omrani, M.D. (2017). Association of MiR-146a Expression and Type 2 Diabetes Mellitus: A Meta-Analysis. Int. J. Mol. Cell. Med. *6*, 156–163.
38. Ding, X., Jian, T., Wu, Y., Zuo, Y., Li, J., Lv, H., Ma, L., Ren, B., Zhao, L., Li, W., and Chen, J. (2019). Ellagic acid ameliorates oxidative stress and insulin resistance in high glucose-treated HepG2 cells via miR-223/keap1-Nrf2 pathway. Biomed. Pharmacother. *110*, 85–94.
39. Jampoka, K., Muangpaisarn, P., Khongnomnan, K., Treeprasertsuk, S., Tangkijvanich, P., and Payungporn, S. (2018). Serum miR-29a and miR-122 as Potential Biomarkers for Non-Alcoholic Fatty Liver Disease (NAFLD). MicroRNA *7*, 215–222.
40. Yu, F., Wang, X., Zhao, H., Hao, Y., and Wang, W. (2019). Decreased Serum miR-1296 may Serve as an Early Biomarker for the Diagnosis of Non-Alcoholic Fatty Liver Disease. Clin. Lab. *65*.
41. He, Z., Yang, J.J., Zhang, R., Li, H.T., Wu, L., Jiang, F., Jia, W.P., and Hu, C. (2019). Circulating miR-29b positively correlates with non-alcoholic fatty liver disease in a Chinese population. J. Dig. Dis. *20*, 189–195.
42. Zong, Y., Yan, J., Jin, L., Xu, B., He, Z., Zhang, R., Hu, C., and Jia, W. (2020). Relationship between circulating miR-132 and non-alcoholic fatty liver disease in a Chinese population. Hereditas *157*, 22.
43. Jiang, H., Qian, Y., Shen, Z., Liu, Y., He, Y., Gao, R., Shen, M., Chen, S., Fu, Q., and Yang, T. (2021). Circulating microRNA-135a-3p in serum extracellular vesicles as a potential biological marker of non-alcoholic fatty liver disease. Mol. Med. Rep. *24*, 498.
44. Duan, Y., Pan, X., Luo, J., Xiao, X., Li, J., Bestman, P.L., and Luo, M. (2022). Association of Inflammatory Cytokines With Non-Alcoholic Fatty Liver Disease. Front. Immunol. *13*, 880298.
45. Gedebjerg, A., Bjerre, M., Kjaergaard, A.D., Nielsen, J.S., Rungby, J., Brandslund, I., Maeng, M., Beck-Nielsen, H., Vaag, A., Sørensen, H.T., et al. (2023). CRP, C-Peptide, and Risk of First-Time Cardiovascular Events and Mortality in Early Type 2 Diabetes: A Danish Cohort Study. Diabetes Care *46*, 1037–1045.

STAR★METHODS

KEY RESOURCES TABLE

REAGENT or RESOURCE	SOURCE	IDENTIFIER
Antibodies		
Rabbit anti-FASN antibody	Proteintech, USA	RRID: AB_2100801
Rabbit anti-FOXO1 antibody	Cell Signaling Technology, USA	RRID: AB_2106495
Rabbit anti-SCD antibody	Abcam, UK	RRID: AB_2928123
Rabbit anti-FABP1 antibody	Abcam, UK	RRID: AB_11143760
Rabbit anti-HMGCR antibody	Proteintech, USA	RRID: AB_2877957
Rabbit anti-PARP antibody	Cell Signaling Technology, USA	RRID: AB_659884
Rabbit anti-cleaved PARP antibody	Cell Signaling Technology, USA	RRID: AB_10699459
Rabbit anti-Caspase 3 antibody	Cell Signaling Technology, USA	RRID: AB_2069872
Rabbit anti-cleaved Caspase 3 antibody	Cell Signaling Technology, USA	RRID: AB_2341188
Rabbit anti-JNK antibody	Cell Signaling Technology, USA	RRID: AB_2250373
Rabbit anti-phosphorylated JNK antibody	Cell Signaling Technology, USA	RRID: AB_823588
Mouse anti-GAPDH antibody	Proteintech, USA	RRID: AB_2107436
Rabbit anti-F4/80 antibody	Cell Signaling Technology, USA	RRID: AB_2799771
Rabbit anti-Ly6G antibody	Cell Signaling Technology, USA	RRID: AB_2909808
Rabbit anti-αSMA antibody	Cell Signaling Technology, USA	RRID: AB_2734735
Peroxidase AffiniPure Goat Anti-Rabbit IgG	Jackson immunoresearch, USA	RRID: AB_2313567
Peroxidase AffiniPure Goat Anti-Mouse IgG	Jackson immunoresearch, USA	RRID: AB_10015289
IHC Detection Reagent (HRP, Rabbit)	Cell Signaling Technology, USA	RRID: AB_10544930
Chemicals, peptides, and recombinant proteins		
Sodium pyruvate	J&K Scientific, China	Cat# P2256
Sodium lactate	Leagene, China	Cat# 1614308
Streptozotocin	Leagene, China	Cat# V900890
Sodium palmitate	Sigma-Aldrich, USA	Cat# P9767
Critical commercial assays		
Triglyceride detection kit	Nanjing Jiancheng, China	Cat# A110-1
Total cholesterol detection kit	Nanjing Jiancheng, China	Cat# A111-1
Oligonucleotides		
miR-337-3p	Shanghai GenePharma, China	N/A
miR-337-3p-MUT	Shanghai GenePharma, China	N/A

RESOURCE AVAILABILITY

Lead contact

Further information and requests for resources and reagents should be directed to and will be fulfilled by the lead contact, Jing Chen (jingchen@simm.ac.cn).

Materials availability

This study did not generate new unique reagents.

Data and code availability

- Data reported in this paper will be shared by the lead contact upon request.
- This paper does not report original code.
- Any additional information required to reanalyze the data reported in this paper is available from the lead contact upon request.

EXPERIMENTAL MODEL AND STUDY PARTICIPANT DETAILS

Cell lines

HepG2, HEK293 and 293T cell lines were all purchased from American Type Culture Collection. HepG2 cells were maintained in MEM (HyClone, USA) containing 10% fetal bovine serum (FBS; Gibco, USA) and 1% antibiotic-antimycotic (Thermo Fisher Scientific, USA) at 37°C with 5% CO_2. HEK293 and 293T cells were maintained in DMEM (Gibco, USA) containing 10% FBS (Gibco, USA) and 1% antibiotic-antimycotic (Thermo Fisher Scientific, USA) at 37°C with 5% CO_2. L02 cells were maintained in RPMI-1640 (Gibco, USA) containing with 10% FBS (Gibco, USA) and 1% antibiotic-antimycotic (Meilunbio, China) at 37°C with 5% CO_2.

Animal experiments

All animal experiments complied with the Institutional Ethical Guidelines and were approved by the Institutional Animal Care and Use Committee, Shanghai Institute of Materia Medica, Chinese Academy of Sciences (2019-04-RJ-191 for HFHC diet-induced mouse model, 2020-04-RJ-213 for the miR-337-3p-overexpressing GAN diet-induced mouse model, and 2022-01-RJ-266 for the miR-337-3p-overexpressing STZ mouse model).

HFHC diet-induced mouse model

db/db mice (male, aged 8 weeks) were purchased from GemPharmatech Co.,Ltd (China) and fed with a high-fat/cholesterol diet(71.5% Purina Rodent Chow; 0.5% Cholesterol; 5% Fructose; 11.5% Coconut Oil; 11.5% Corn Oil by weight. Research Diets, USA) or a normal control diet. After 20 weeks, the mice were sacrificed and the livers were collected for subsequent analysis.

MiR-337-3p-overexpressing GAN diet-induced mouse model

C57/BL6J mice (male, aged 8 weeks) were purchased from Shanghai Jihui Laboratory Animal Care Co.,Ltd (China). After 3 weeks of feeding with Gubra-Amylin NASH (GAN) diet (2% cholesterol by weight and 40% of calories derived from fat, 20% from fructose, Research Diets, USA), mice were injected with 200μl of 5×10^12 vector genomes per ml (vg/ml) AAVs via the tail vein, in which GPAAV-Mcherry was mCherry group (n=10/group) and GPAAV-Mcherry-mmu-miR-337-3p was the miR-337-3p group (n=10/group). That is to say, the virus titer was 1×10^12 per mouse.The mice in the two groups continued to be fed with GAN diet and were sacrificed at 14 weeks post-injection. To verify the model was established successfully, we also set up a normal chow diet group (NCD) transfected with the AAV of mcherry, which were sacrificed at the same time with GAN diet mice.

MiR-337-3p-overexpressing HFD/STZ-induced mouse model

C57/BL6J mice (male, aged 8 weeks) were purchased from Beijing Vital River Laboratory Animal Technology (Beijing, China). Mice were injected with 200μl of 5×10^12 vector genomes per ml (vg/ml) AAVs via the tail vein, in which GPAAV-Mcherry was the mCherry group (n=9/group) and GPAAV-Mcherry-mmu-miR-337-3p was the miR-337-3p group (n=9/group). The mice were all fed with high fat diet (60 kcal% Fat, Research Diets, USA) and were injected with streptozocin (STZ, 100mg/kg) at Day 40 and 96. Then, the mice in the two groups were sacrificed at Day 114 post-injection of AAVs. Finally, the liver and serum samples were collected for subsequent analysis.

METHOD DETAILS

Adeno-associated virus construction

The plasmid (GPAAV-Mcherry-mmu-miR-337-3p) in the AAV2/8 delivery system which overexpressed miR-337-3p in the mouse liver was constructed by Genomeditech (Shanghai, China), in which pri-miR-337 was cloned into the vector. The control was served by an empty adeno-associated virus (GPAAV-Mcherry).

AAV packaging was initiated from the co-transfection of GPAAV-Mcherry-mmu-miR-337-3p (or GPAAV-Mcherry), pHelper and pAAV2/8 (1:1:1) for 72h in 293T cells using calcium phosphate transfection kit. AAV purification was performed as previously described.[20] Briefly, PEG 8000 (10%) and NaCl (1M/l) were used to collect the virus through the cells which were cultured for 3 days to produce the virus.

The lysis buffer was consist of 50mM Tris-HCl, 150mM NaCl, 2mM $MgCl_2$, pH8.0. The sediment was resuspended in this lysis buffer.Some residual DNA were cleared by Benzonase (50U/ml). The mature virus was enriched using an ultrafiltration column (100 KD).

Oral glucose tolerance tests (OGTT) and pyruvate-tolerance test (PTT)

In OGTT and PTT assay, mice were fasted overnight and orally administered glucose (1.5g/kg body weight) or intraperitoneally injected with pyruvate (1.5g/kg body weight). For all tests, the blood glucose concentrations were measured at 0, 15, 30, 45, 60, 90, and 120 min using a portable glucose meter (Roche, Switzerland).

Primary mouse hepatocytes culture

Primary mouse hepatocytes were isolated from healthy mice. The liver was perfused with solution I (0.5mM EGTA) and solution II (DMEM, 0.2mg/ml Collagenase Type IV (Sigma, USA)) in order. Then, the liver sac was cut to release the hepatocytes in DMEM (Gibco, USA). Those

hepatocytes were resuspended with 45% percoll and spined at 1500rpm for 8min. Finally, the cells were cultured in William's E (10% FBS, 1% antibiotic-antimycotic, 1% Glutamine, 1% ITS (Thermo Fisher Scientific)) for further experiments.

Plasmids construction

HMGCR 3'UTR sequence (NCBI Reference Sequence: NM_000859.3, 1759bp) was amplified from the cDNAs of HepG2 cells, and inserted into the psi-Check2 (Addgene, China) at the XhoI and BamH1 restriction sites.

Luciferase assay

HEK293 cells were transfected with the luciferase reporter plasmid (*HMGCR* 3'UTR (100ng/well)) with miR-337-3p or miR-337-3p-MUT(MUT) (GenePharma, China) by using Lipofectamine 2000 (Thermo Fisher Scientific, USA) in 96-well plates. At 24 h later, those cells were lysed to examine luciferase activity following a dual-luciferase reporter assay system, in which luciferase activity (L) normalized to firefly Renilla luciferase activity (R) stood for the activity of *HMGCR* 3'UTR.

Western blot analysis

The cell lysis buffer were consist of 1M Tris, pH 7.6, 1M NaCl, 1% NP40, 5% sodium deoxycholate, proteinase inhibitor (cocktail, Thermo Fisher Scientific). The protein of mouse liver tissues and HepG2 which were transfected with miR-337-3p/NC were released by the cell lysis buffer. And those protein were quantified with BCA Protein Assay Kit (Pierce, Thermo Fisher Scientific).Then the proteins were separated by electrophoresis in 10% SDS-PAGE and then electro-transferred to PVDF membranes (Millipore, USA). After blocking with 5% non-fat milk in TBST, the protein bands were incubated with the following primary antibodies: anti-FASN (1:2000, ProteinTech, USA), anti-FOXO1 (1:1000, ProteinTech, USA), anti-SCD (1:20000, ProteinTech, USA), anti-FABP1 (1:2000, Abcam, UK), anti-PARP (1:1000, Abcam, UK), anti-cleaved PARP (1:1000, Abcam, UK), anti-Caspase 3 (1:1000, CST, USA), anti-cleaved Caspase 3 (1:1000, CST, USA), anti-HMGCR (1:1000, Abcam, UK), anti-JNK (1:1000, ProteinTech, USA) or anti-p-JNK (1:1000, ProteinTech, USA) at 4°C overnight, then incubated with secondary antibodies at room temperature for 1 h, and finally visualized using a Lumi Q ECL reagent solution kit (Share-Bio, China) according to the manufacturer's instructions. GAPDH was used as the internal loading control.

Real-time quantitative PCR analysis

The trizol reagent (Takara, Japan) were used to release total RNAs of liver tissues and HepG2 cells. To detect related mRNA, the cDNA was reversed-transcribed using PrimeScriptTM RT Master Mix (Takara). For the detection of related miRNAs, we used TaqMan MicroRNA Reverse Transcription Kit (Thermo Fisher Scientific) for the reverse transcription. RT-PCR was performed using the 7500 Fast Real-Time PCR System (7500 Software v2.0.5, Applied Biosystems) with SYBR Premix Ex TaqTM (Yeason, China) for genes and TaqMan Universal Master Mix II for miRNAs. GAPDH was used to normalize all genes' expression., while U6 was used to normalize miRNA levels. All oligonucleotide primers were synthesized by Biosune (Shanghai, China) and the sequences were listed in Table 1. Probes for miRNAs (U6 snRNA (001973), mmu-miR-337-3p (472163), hsa-miR-337-3p (478035)) were obtained from Thermo Fisher Scientific.

Staining of liver sections

HE staining

The slides were deparaffinized through Xylene and EtOH, then blocked by the hematoxylin for 5 min at room temperature (RT). Next, they were washed with distilled water for 2 times (3 min per time with 1% hydrochloric acid ethanol solution) and blocked in 0.5% eosin for 3 min followed by another washing with distilled water for 2 min. Finally, they were dehydrated and sealed.

PAS staining

The slides were deparaffinized through Xylene and EtOH, then washed with distilled water for 3 min. Next, they were blocked by periodate alcohol solution for 10 min and washed with distilled water for 3 min. After that, they were blocked with the Schiff solution and washed with distilled water for 2 min. Finally, they were dehydrated and sealed.

Immunohistochemical staining

The slides were deparaffinized through Xylene and EtOH, then recovered antigen by heating them in citrate buffer for 10 min. After blocked in 3% hydroperoxide in PBS for 15 min at RT, the slides was blocked in 3% normal goat serum for 1h and incubated in the humidified chamber for 1h at RT. Next, the slides were added with primary antibody Ly6G(1:400, CST, USA), α-SMA(1:400, CST, USA) or F4/80(1:1000, CST, USA), second antibody, DAB substrate and hematoxylin in order. Finally, they were dehydrated and sealed.

Oil Red O staining

The frozen liver sections in slides were washed with 60% isopropanol for 30s and stained with Oil Red O (Sigma, USA) solution (in 60% isopropanol) for 25min followed by washing with PBS for 30s. In the end, the tissue sections were stained with hematoxylin for 10s. For the Oil Red O staining in cell, the cell was fixed with 4% paraform for 10 min and staining in Oil Red O solution for 30 min, then washed with

60% isopropanol twice. To quantify Oil Red O content levels, 100μl isopropanol was added to each well. After shaking at room temperature for 5min, the absorbance was read at 490nm. Meanwhile cell viability as a normalization control was detected by CCK-8 assay kit.

Sirius Red staining

The slides were deparaffinized through Xylene and EtOH. Then, the slides were stained by Sirius Red solution (Jiancheng, Nanjing) for 30 min. At last, the slides were stained by hematoxylin solution (Jiancheng, Nanjing) for 30s.

Biochemical analysis

The blood of mice was centrifuged at 1000g for 3 minutes to obtain serum. The TC and LDLC in serum were Tdetermined by enzyme colorimetric method. The ALT and ALP in serum were tested via ALT activity detection kit (Roche, Switzerland) and ALP activity detection kit (Roche, Switzerland). The liver tissues or cells were lysed by 1% trition for 30 min, and the TG or TC contents were detected by TG or TC assay kit (Jiancheng, Nanjing).

Mass spectrometry (MS)

Cells transfected with miR-337-3p or negative control (NC) were lysed in the SDT lysis buffer. All experiments were performed on an Q Exactive HF-X mass spectrometer with a nanoLC easy1200 (Thermo Fisher Scientific). Peptides were loaded on a self-packed column (75 μm × 150 mm, 3 μm ReproSil-Pur C18 beads, 120 Å, Dr. Maisch GmbH, Ammerbuch, Germany) and separated with a 90 min gradient at a flow rate of 300 nL/min. Solvent A was 0.08% formic acid in water; solvent B was 80% acetonitrile, and 0.08% formic acid. The Q Exactive HFX was programmed in the data-dependent acquisition mode. An MS1 survey scan of 350–1700 m/z in the Orbitrap at a resolution of 120,000 was collected with an AGC target of 3e6 and maximum injection time of 50 ms. Precursor ions were filtered according to monoisotopic precursor selection, charge state (+ 2 to + 6), and dynamic exclusion (40 s with a ±10 ppm window). Then, the top 20 most intense precursors were subjected to HCD fragmentation. The instrument parameters were set as follows: 32% normalized collision energy, 45,000 resolution, 100,000 AGC target, 120 ms maximum injection time, 105 Da first mass, 1 m/z isolation width. And the data of MS were processed by searching against the UniProt/SwissProt Human database via Maxquant (1.6.5.0), with default settings for 6-plex TMT quantification. Trypsin/P was selected as the digestive enzyme with allowance of one missed cleavage. Minimum 7 amino acids for peptide, >2 peptides were required per protein. For peptide and protein identification, false discovery rate (FDR) was set to 1%. TMT reporter ion intensity was used for quantification.

CRISPR/Cas9-mediated knockout of miR-337-3p

Two single-guide RNAs (sgRNAs, 5′-CACCGTCTGCACCCTTGGCTGCACG-3′, 5′-CACCGGCAAGCGCTCGGATGGCAGA-3′) were cloned into px330-mCherry and px330-GFP vectors, respectively. These two plasmids were co-transfected into L02 cells for 48 h, and the double-positive cells were sorted by the flow cytometry. Clones derived from double-positive cells were analyzed using qPCR to confirm the knockout of miR-337-3p. Single cell co-transfected with px330-mCherry and px330-GFP empty vectors were used as wild-type L02 cell.

QUANTIFICATION AND STATISTICAL ANALYSIS

Data were analyzed by using GraphPad Prism software. The data of *in vitro* experiments were displayed as the mean ±SD and those of *in vivo* experiments were displayed as the mean ± SEM.[34] Significance was determined by Student's two-tailed t-test. Linear relationship was presented as Pearson correlation coefficients. *p <0.05, **p <0.01, ***p <0.001 as indicated.